



Martensitic transformation in a B2-containing CuZr-based BMG composite revealed by *in situ* neutron diffraction[☆]



Gian Song^{a, c, *}, Chanhoo Lee^a, Sung Hwan Hong^b, Ki Buem Kim^b, Shuying Chen^a, Dong Ma^c, Ke An^c, Peter K. Liaw^{a, **}

^a Department of Materials Science and Engineering, The University of Tennessee, Knoxville, TN 37996-2200, USA

^b Faculty of Nanotechnology and Advanced Materials Engineering, Sejong University, Gwangjin-gu, Seoul, 143-747, South Korea

^c Chemical and Engineering Materials Division, Oak Ridge National Laboratory, Oak Ridge, TN 37831, USA

ARTICLE INFO

Article history:

Received 28 March 2017

Received in revised form

24 May 2017

Accepted 24 June 2017

Available online 27 June 2017

Keywords:

Metallic glass

Composite

Deformation

Martensitic transformation

Neutron diffraction

ABSTRACT

CuZr-based bulk-metallic-glass (BMG) composites reinforced by a B2-type CuZr crystalline-phase (CP) have been widely studied, and exhibit that the plastic deformation of the CP induces martensitic transformation from the B2 to B19', which plays a dominant role in the deformation behavior and mechanical properties. In the present study, 2.0% Co containing CuZr-based BMG composites were investigated using in-situ neutron-diffraction technique. The in-situ neutron-diffraction results reveal the continuous load transfer from the glass matrix to B2 CP and martensitic transformation from the B2 CP to B19' during the deformation of the composite. Moreover, it was found that the martensitic transformation is initiated at the applied stress higher than 1500 MPa, and is significantly suppressed during the deformation, as compared to other 0.5% Co-containing CuZr-based BMG composites. Based on these in-situ neutron-diffraction results, the martensitic transformation is strongly affected by the amount of the addition of Co, which determines the mechanical properties of CP-reinforced BMG composites, such as ductility and hardening capability.

© 2017 Elsevier B.V. All rights reserved.

1. Introduction

Bulk metallic glass (BMG) has received extensive attention as promising structural materials due to unique properties [1–4]. However, the poor plasticity comes from the localized deformation in shear bands, which leads to catastrophic failure [5,6]. One of the most effective approaches to improve the plastic deformability is to introduce a crystalline inclusion (reinforcement) [7–10]. This

crystalline inclusion is known to be effective to hinder the propagation of shear bands and facilitate the formation of multiple shear bands, thus, improve the plastic deformability. For example, crystalline-phase (CP) reinforced BMG composites exhibit the typical dislocation-slip deformation in the crystalline phase and accommodation of shear-banding strains in the glassy matrix, which plays a dominant role in enhancing the plasticity [8,10]. However, the limited plastic deformability under tension has been observed due to work softening that leads to necking in the early stage of plastic deformation, which restricts their application as structural engineering materials [9,11].

Recently, significant improvement in the work hardenability and plastic deformability under compression and tension has been observed in BMG composites reinforced by B2 and β -Ti CPs [10,12–17]. It has been reported that the improved plasticity and strain hardening are strongly associated with the deformation-induced phase transformation in the CPs, such as martensitic transformation from a B2 to monoclinic B19' CPs in CuZr- and TiCu-based BMG composites [12,17]. It is generally postulated that the martensitic transformation is initiated when the B2-CuZr CP starts deforming plastically, and both the plastic deformation of the soft

[☆] This manuscript has been authored by UT-Battelle, LLC under Contract No. DE-AC05-00OR22725 with the U.S. Department of Energy. The United States Government retains and the publisher, by accepting the article for publication, acknowledges that the United States Government retains a non-exclusive, paid-up, irrevocable, worldwide license to publish or reproduce the published form of this manuscript, or allow others to do so, for United States Government purposes. The Department of Energy will provide public access to these results of federally sponsored research in accordance with the DOE Public Access Plan (<http://energy.gov/downloads/doe-public-access-plan>).

^{*} Corresponding author. Chemical and Engineering Materials Division, Oak Ridge National Laboratory, Oak Ridge, TN 37831, USA.

^{**} Corresponding author.

E-mail addresses: gsong1@utk.edu (G. Song), pliaw@utk.edu (P.K. Liaw).

B2-CuZr CP and the martensitic transformation should play a direct role in the macroscopic plastic deformation behavior of the composites. This transformation might be responsible for the enhanced strain hardening and suppression of early necking during plastic deformation, and, thus, result in the considerable tensile ductility [18,19]. Moreover, the martensitic transformation behavior of the B2 CPs on the work hardening stage has been systematically investigated in Ti-based BMG composite containing B2 CPs [20,21]. The phase transformation from B2 to B19' CPs occurred firstly at the vicinity of interface between amorphous matrix and B2 CPs and gradually progressed into inside B2 CPs with increasing strain [21]. The martensitic transformed regions in B2 CPs revealed a higher hardness value in comparison with the inside regions maintaining B2 structure [20]. This previous observation can be considered as an evidence that the work hardening of B2 CPs-reinforced BMG composites is deeply dependent on martensitic transformation of B2 CPs during deformation.

In the present study, we present a systematic investigation regarding dynamic evolution of elastic/plastic response of constitutive phases in CuZr-CP reinforced BMG composites consisting of 2.0% Co by state-of-the-art neutron diffractometer, VULCAN Engineering Materials Diffractometer at the Spallation Neutron Source (SNS), Oak Ridge National Laboratory (ORNL) [22–24]. The in-situ neutron diffraction technique provides governing deformation mechanisms of engineering materials, such as elastic/plastic anisotropy between constitutive phases/intergranular grains, and deformation mechanism transition [25–29]. The present elastic/plastic response of the CuZr CP during compression deformation reveals that the reinforcing CuZr CP assumes additional load transferred from the glassy matrix. Furthermore, the martensitic transformation is considerably suppressed as compared to 0.5% Co containing CuZr-CP reinforced BMG composites, which is strongly associated with mechanical properties, such as work hardening behavior of the composite. The objective of the present study is to provide a comprehensive understanding of the effect of the Co addition and martensitic transformation on the microscopic- and macroscopic-deformation behavior, hence the mechanical properties in CP reinforced BMG composites that undergo the martensitic transformation.

2. Methods

2.1. Materials and microstructural characterization

The nominal composition of the alloy investigated in the present study is $\text{Cu}_{47}\text{Zr}_{47}\text{Al}_4\text{Co}_2$ in atomic percent (at. %). The Cu-Zr-Al-Co bulk metallic glass (BMG) composites were prepared by arc melting of the pure elements under an argon atmosphere followed by direct casting into cylindrical rods with 3 mm diameter and 50 mm length using a suction casting facility. The casting facility is equipped with temperature-controllable cooling system, which allows for microstructural manipulation by introducing different cooling rates. Using the cooling system, two specimens with different volume fractions of the crystalline B2-phase were fabricated. Scanning-electron microscopy (SEM: JEOL JSM-6390) equipped with an energy-dispersive X-ray spectrometer (EDS) was used for microstructure observation.

2.2. In-situ neutron-diffraction experiments

In-situ neutron-diffraction (ND) compression tests at room temperature were carried out using the VULCAN Engineering Diffractometer at the SNS, ORNL [22]. The ND instrument utilizes time-of-flight (TOF) measurements, in which the incident beam is polychromatic with a range of wave length, which allows for the ND

measurements with a diffraction pattern covering a wide range of d-spacing without rotation of samples or detectors. The wave length of the neutron can be manipulated by the frequency of chopper and 30 Hz of frequency was utilized, which selects d-spacing ranging approximately from 0.8 to 2.5 Å.

A schematic of the ND experimental setup is presented in Fig. 1(a). Two detectors, designated Bank 1 and 2, which are fixed at an angle of 45° to the loading direction, were employed to collect diffracted beam from polycrystalline grains with lattice planes parallel to the axial and transverse directions, respectively. The cube in Fig. 1(a) represents the sample volume illuminated by the neutron beam, which is defined by the beam slit and the collimator used. In the current setup, the size of the slit and collimator is $3 \times 3 \text{ mm}^2$ and 2 mm, respectively, which provides an illuminated volume of $\sim 18 \text{ mm}^3$ in the tested specimens. Fig. 1(b) shows a compression specimen with a diameter of 3 mm and a length of 7.5 mm, which was mounted on the load frame. The compression specimen ratio of 2.5 was utilized to secure the higher volume of sample illuminated and reduce the diffracted beam that is blocked by the sample-holding platens. Due to the absence of a room-temperature extensometer for the small size sample, the cross-head displacement was used to obtain the macroscopic strain at room temperature. Even though the crosshead displacement is not accurate to measure the macroscopic strain, the macroscopic yield stress can be clearly observed as the deviation from elastic linear response in the stress versus displacement curves.

For the measurement of the lattice strain, a constant load control mode was employed with stepwise-loading steps. Neutron diffraction data were collected over a period of 30 min at each stress level. Above a stress level close to 1800 MPa, a constant displacement control mode was utilized with an incremental step of 0.002–0.005 mm, and neutron data were collected at each step for 30 min. ND measurements were conducted during both loading and unloading after plastic deformation of 1.5%. During the unloading, the sample was measured in a stepwise-unloading mode.

Since the Cu-Al-Zr-Co BMG composite only consists of a B2-CuZr CP embedded in the amorphous matrix, the (hkl) plane spacings of the B2 phase were determined from a single peak fitting approach employing VULCAN Data Reduction and Interactive Visualization software (VDRIVE) [30]. The (hkl) plane-specific lattice strains represent the lattice strain of the individual grain of the B2 phase, which depends on the elastic and plastic anisotropy of the individual grains. The (hkl) plane-specific lattice strains are calculated using the following formula

$$\varepsilon_{hkl} = (d_{hkl} - d_{hkl}^0) / d_{hkl}^0 \quad (1)$$

where ε_{hkl} is the lattice strain in the (hkl)-oriented grains, d_{hkl}^0 is the reference (hkl) lattice spacing before loading and d_{hkl} is the (hkl) lattice spacing as a function of compressive stress or displacement.

3. Results

Fig. 2(a) and (c) show SEM images of the $\text{Cu}_{47}\text{Zr}_{47}\text{Al}_4\text{Co}_2$ BMG composites with different crystalline-volume fractions. The dark-contrast crystalline phase is embedded in the bright glassy matrix and the (a) $\text{Cu}_{47}\text{Zr}_{47}\text{Al}_4\text{Co}_2$ BMG composite contains the higher volume fraction (HVF) of the crystalline phase [75–85 vol percent (vol. %)], compared to (c) that with the lower volume fraction (LVF) of the crystalline phase (45–55 vol %). Energy-dispersive X-ray spectroscopy (EDS) was conducted on the crystalline and glassy phases, and the compositions are summarized in Table 1. The composition of the crystal phase is similar to that of the glassy

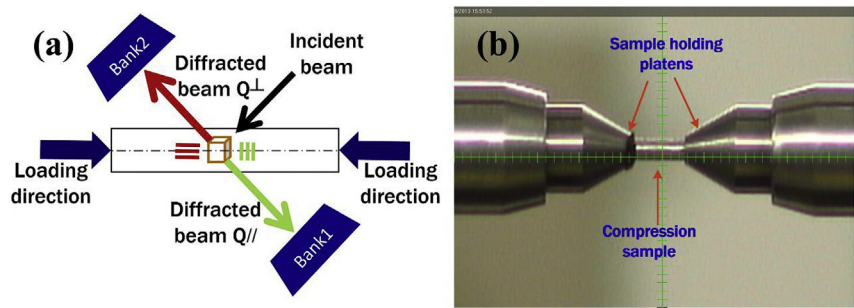


Fig. 1. (a) A schematic illustrating geometric arrangement of the in-situ compression experiment using neutron diffraction (b) a photograph showing a compression sample loaded on the platens.

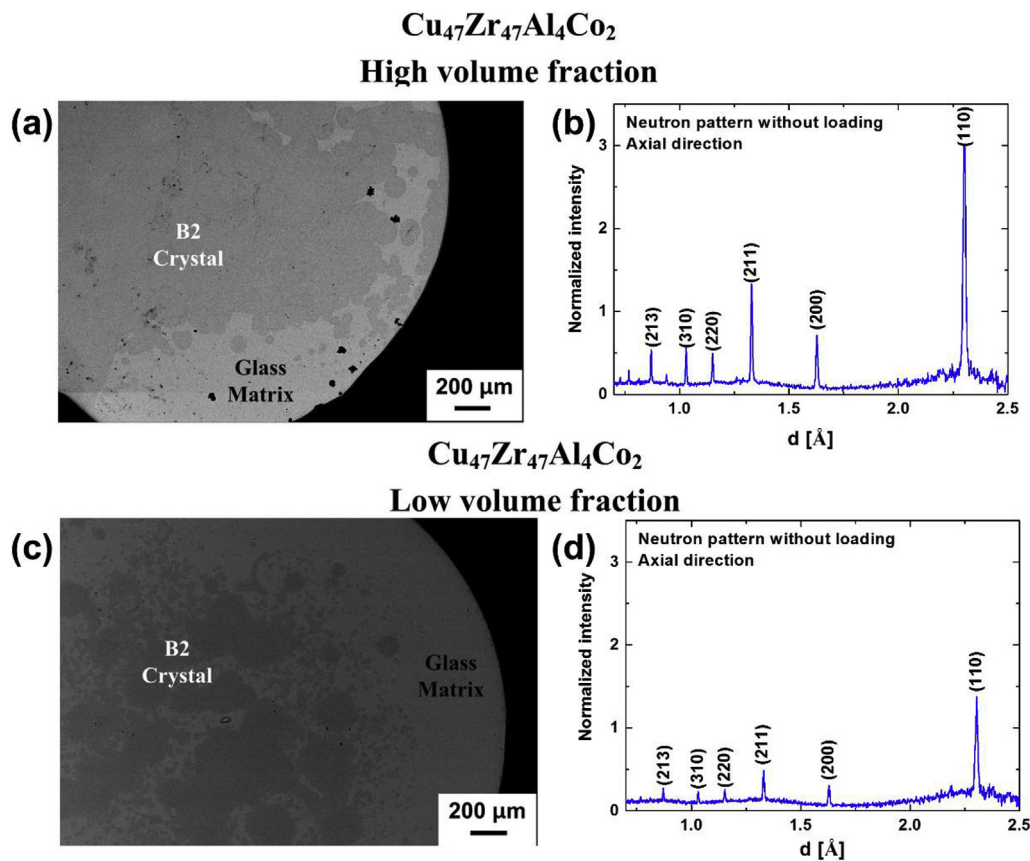


Fig. 2. (a)–(c) Scanning-electron microscopy (SEM) images and (b)–(d) neutron diffraction (ND) patterns of the Cu₄₇Zr₄₇Al₄Co₂ BMG composites with (a)–(b) high volume fraction and (c)–(d) low volume fraction of the B2 crystalline phase, respectively. These SEM and ND patterns are obtained before the compression loading.

matrix for both HVF and LVF BMG composites, and their compositions are close to the B2-type CuZr phase with a minor addition of Al and Co. Moreover, the compositions of the crystal and glass matrix phases between HVF and LVF BMG composites are more or

Table 1
Scanning-electron microscopy (SEM) energy-dispersive spectroscopy (EDS) results in atomic percent (at. %). The uncertainties for the EDS results are represented by the standard deviation from the measurement series.

Materials	Phase	Cu	Zr	Al	Co
HVF	Crystal	46.9 ± 0.3	47.0 ± 0.2	4.1 ± 0.2	1.9 ± 0.2
	Glass	46.9 ± 0.2	46.9 ± 0.3	4.1 ± 0.2	2.1 ± 0.1
LVF	Crystal	46.4 ± 0.2	47.4 ± 0.3	4.4 ± 0.1	1.9 ± 0.1
	Glass	46.5 ± 0.3	47.2 ± 0.3	4.3 ± 0.2	1.9 ± 0.1

less identical. Fig. 2(b) and (d) present the neutron-diffraction (ND) patterns for the (b) HVF and (d) LVF BMG composites before loading, respectively. All ND patterns contain a broad and diffuse diffraction background at d-spacing ranging from 2 to 2.5 Å, which indicates the presence of an amorphous phase in both specimens. It can be noticed that the intensity of crystalline peaks is proportional to their volume fractions. The main sharp diffraction peaks in Fig. 2(b) and (d) are identified as the B2 structure CuZr phase (*Pm*-3m). The lattice parameter for each (hkl) plane was determined from the ND patterns using a single peak fitting approach, and the lattice parameters from the peaks observed in each ND pattern were averaged. The calculated average-lattice parameters are listed in Table 2. The lattice parameters of the B2-CuZr phase for both samples are more or less identical regardless of the directions.

Table 2

The lattice parameters of the B2 crystalline phase along the axial and transverse directions of the HVF and LVF BMG composites, determined using a single peak fitting approach.

	Direction	HVF	LVF
Lattice parameter (Å)	Axial	3.2516 (± 0.0003)	3.2549 (± 0.0005)
	Transverse	3.2507 (± 0.0004)	3.2507 (± 0.0006)

Fig. 3 displays the engineering stress vs. strain curves during the in-situ compression tests for the (a) HVF and (b) LVF BMG composites, respectively. A linear elastic regime is clearly observed, followed by a transition to a plastic regime, as noticed by the deviation from the linear gradient. As depicted in Fig. 3(a) and (b), the ND measurement mode was shifted from constant load to displacement-control modes at a stress level close to 1800 MPa. Due to the absence of a room-temperature extensometer, the stress-strain curves show extended elastic strain and low Young's modulus. Even though the Young's modulus cannot be accurately measured, an attempt to obtain the yield stress of each sample was made using 0.2% offset approach. The yield strength (1780 MPa) of

the HVF BMG composite is slightly lower than that (1900 MPa) of the LVF BMG composite. After yielding, the LVF BMG composite exhibits limited work hardening behavior, followed by saturated flow-stress with increasing the plastic strain [Fig. 3(b)]. However, HVF BMG composite seems to show more pronounced work hardening behavior than the LVF BMG composite [Fig. 3(a)]. After the plastic strain, the HVF BMG composite was unloaded down to near-zero stress level in stepwise-unloading mode [Fig. 3(a)], while the LVF BMG composite fractured during the further straining [Fig. 3(b)].

Fig. 4 presents the neutron diffraction patterns along the axial (compressive) direction for (a) HVF and (b) LVF BMG composites, captured during the loading and unloading as a function of strain. All the main peaks in the initial stage (without loading) are identified as the B2 CuZr crystalline phase. The neutron patterns in Fig. 4(a) and (b) are obtained from the ND measurements that correspond to red markers in Fig. 3(a) and (b), respectively. For both samples, it is clearly observed that all the (hkl) peaks gradually shift to the lower d-spacing (compressive strain) with an increase of the applied stress, relative to the reference ND patterns (without loading), as indicated by red dotted lines in Fig. 4(a) and (b). After unloading, the peaks shift back to the larger d-spacing, indicating the effect of elastic deformation [Fig. 4(a)]. Interestingly, an additional peak around the d-spacing of 2.05 Å starts to occur for both BMG composites, which corresponds to the (020) peak of martensitic monoclinic CuZr phase [12]. The intensity of the martensitic phase (volume fraction) slightly increases, as the applied stress increases, as denoted by red arrow. The initial stress value for the notable formation of the martensitic phase is lower for HVF BMG composite (1746 MPa) than LVF BMG composite (1946 MPa). Martensitic phase peaks in the transverse direction was not observed at all the applied stresses. After unloading of the HVF BMG composite, the martensitic phase retains with the peak position shifted to the larger d-spacing. It has been reported that there are a specific crystallographic orientation relationship between B2 [(110)_{B2} and (211)_{B2}] and transformed martensitic phases [(020)_{B19'}] [31]. Fig. 4(c) displays the evolution of the intensity of (110)_{B2}, (211)_{B2} and (020)_{B19'} as a function of macroscopic strain of the HVF BMG composite. A subtle variation of the intensity for all the three peaks are observed, which indicates the limited martensitic transformation during the deformation. The linear fitting was conducted on the intensity evolution and reveals a slight reduction of the intensity of the B2 peaks and a modest increase of the martensitic phase.

Fig. 5 presents the evolution of (hkl) plane-specific lattice strains for the B2 phase, defined as Eq. (1), as a function of the applied stress for HVF [(a) and (b)] and LVF [(c) and (d)] BMG composites, respectively. Note that Fig. 5(a) and (c) represent the axial (loading) direction, while Fig. 5(b) and (d) correspond to the transverse direction. Both directions show similar elastic strain evolution except for the smaller lattice strain in the transverse direction due to the Poisson's effect. In the elastic regime of compressive deformation [Fig. 5(a) and (c)], the linear response of the (hkl) plane-specific lattice strains is observed for both specimens. The value of the Young's modulus of the differently-oriented grains (E_{hkl}) is calculated from the measured (hkl) plane-specific lattice strains with the elastic anisotropy factor (A_{hkl}) valid for cubic structures, defined [32,33] as

$$A_{hkl} = \frac{h^2 k^2 + l^2 k^2 + h^2 l^2}{(h^2 + k^2 + l^2)^2} \quad (2)$$

The calculated values of E_{hkl} and A_{hkl} for both samples are summarized in Table 3. The calculated value of E_{hkl} increases with an increment of A_{hkl} , which reflects elastic anisotropy of the B2 CP.

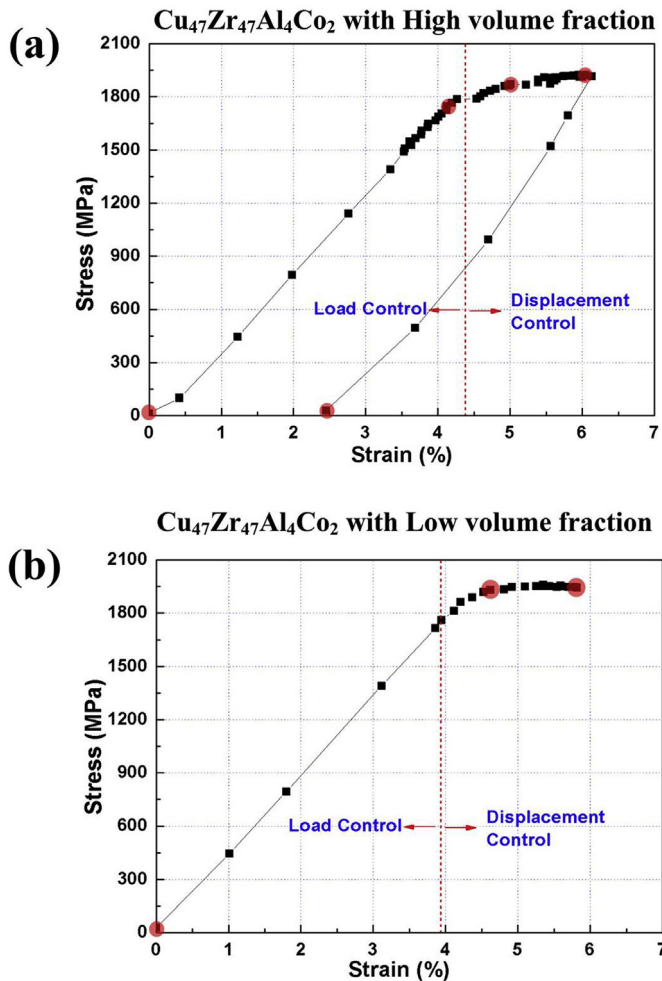


Fig. 3. Stress vs. strain curves recorded during in-situ compression experiments for (a) HVF and (b) LVF BMG composites. The square data points indicate the diffraction data measurements. The measurements were made under load control mode in the elastic regime and displacement control mode in the plastic regime, respectively. The red circle data points correspond to the selected neutron diffraction patterns shown in Fig. 4(c) and (d). (For interpretation of the references to colour in this figure legend, the reader is referred to the web version of this article.)

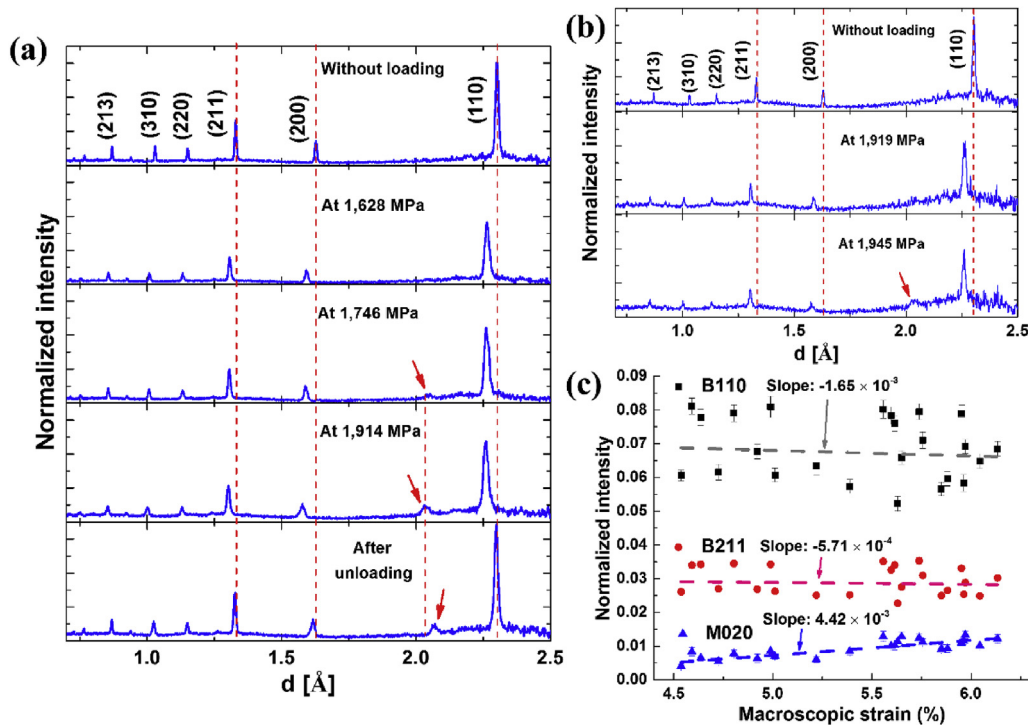


Fig. 4. Diffraction patterns of the (a) HVF and (b) LVF BMG composites, selected from the data points during the compression deformation in Fig. 3(a) and (b), respectively. (c) Evolution of the peak intensity of (110) and (211) for B2, and (020) for B19' as a function of macroscopic strain.

For both directions in Fig. 5[(a)–(d)], the gradients of the specific strains with respect to the applied stress for all the (hkl) planes (diffraction Young's modulus) start to deviate from the linear slope around 1780 MPa for the HVF and 1890 MPa for LVF BMG composites, respectively. The deviation of the lattice strains from the linear slope indicates deformation transition from elastic to plastic regimes, and this transition stress corresponds well with the macroscopic yield stress for both HVF and LVF BMG composites, as observed in Fig. 3(a) and (b). During the plastic deformation, the lattice strain of all the planes continue to increase, which reflects that the B2 phase assumes more load from the glassy matrix. For HVF BMG composite, after unloading, the residual strain of all the planes remain negative (compressive strain) along the loading direction, while the positive residual strain (tensile strain) is captured along the transverse direction. These accumulated strains indicate that the residual strain in the present composite materials is closely associated with the interphase load partitioning between different phases rather than intergranular interaction between differently oriented grains [34]. Interestingly, it is also observed that the gradient of the (110) and (211) lattice planes slightly increases around 1500 MPa, which is lower than the macroscopic yield stress for both axial and transverse directions. This will be discussed in detail in following section.

4. Discussion

The evolution of the lattice strain provides an important information to understand the interaction between constitutive phases and differently-oriented grains in multi-phase materials, such as elastic and plastic anisotropy [35,36]. In elastic deformation range, the linear response of the elastic strain vs. stress curves for all the (hkl) planes of the B2 phase reflects the elastic deformation of the B2 phase. The different linear slopes of the (hkl) planes are caused by the elastic anisotropy in the B2 phase [25,29,37]. When the applied stress approaches the macroscopic yield stress (plastic

deformation), an increase in the gradient relative to the elastic modulus represents plastic yielding of a certain (hkl)-oriented grain (or a phase), whereas a decline of the gradient implies an intergranular (or an interphase) load transfer from the soft grains (which are plastically deforming) to the hard grains (which are elastically deforming). These phenomena are known to be the elastic-plastic anisotropy [38,39]. More detailed description regarding micro-strain evolution can be found in Refs. [28,34]. In the current observation, all the (hkl) lattice strains of the B2 CuZr phase during the macroscopic plastic deformation (higher than 1900 MPa of applied stress) continue to increase without clear load-transfer between them, which indicates that there is no strong interaction (load partitioning) between the differently-oriented grains of the B2 CuZr phase. The decrease in the strain vs. stress slope of the B2 phase is strong evidence supporting the occurrence of the interphase load transfer from the amorphous matrix to the B2 CuZr, as schematically illustrated in Fig. 6(a). Even though the ND cannot detect the elastic or plastic deformation of the amorphous matrix due to the disordered nature, it can be deduced from the lattice strain evolution of the B2 CuZr crystalline surrounded by the amorphous matrix that the amorphous matrix yields by the initiation of shear bands and the additional plastic strain was subsequently transferred to the B2 CuZr phase [19]. Moreover, this interphase load transfer from the amorphous matrix to the CuZr phase can be further supported by the sign of residual strain of the (hkl) oriented grains after unloading, as shown in Fig. 5[(a) and (b)]. The presence of the strengthened B2 phase by the martensitic transformation can effectively hinder the propagation of shear bands, which is another well-known hardening mechanism for CP reinforced BMG composites [40].

The martensite CuZr phase is observed to form at different stresses for the HVF and LVF, and the volume fraction gradually increases with increasing applied stress (strain), as observed in Fig. 4. The stress level at which the martensitic phase first appears in the ND pattern is 1945 MPa for LVF and 1746 MPa for HVF,

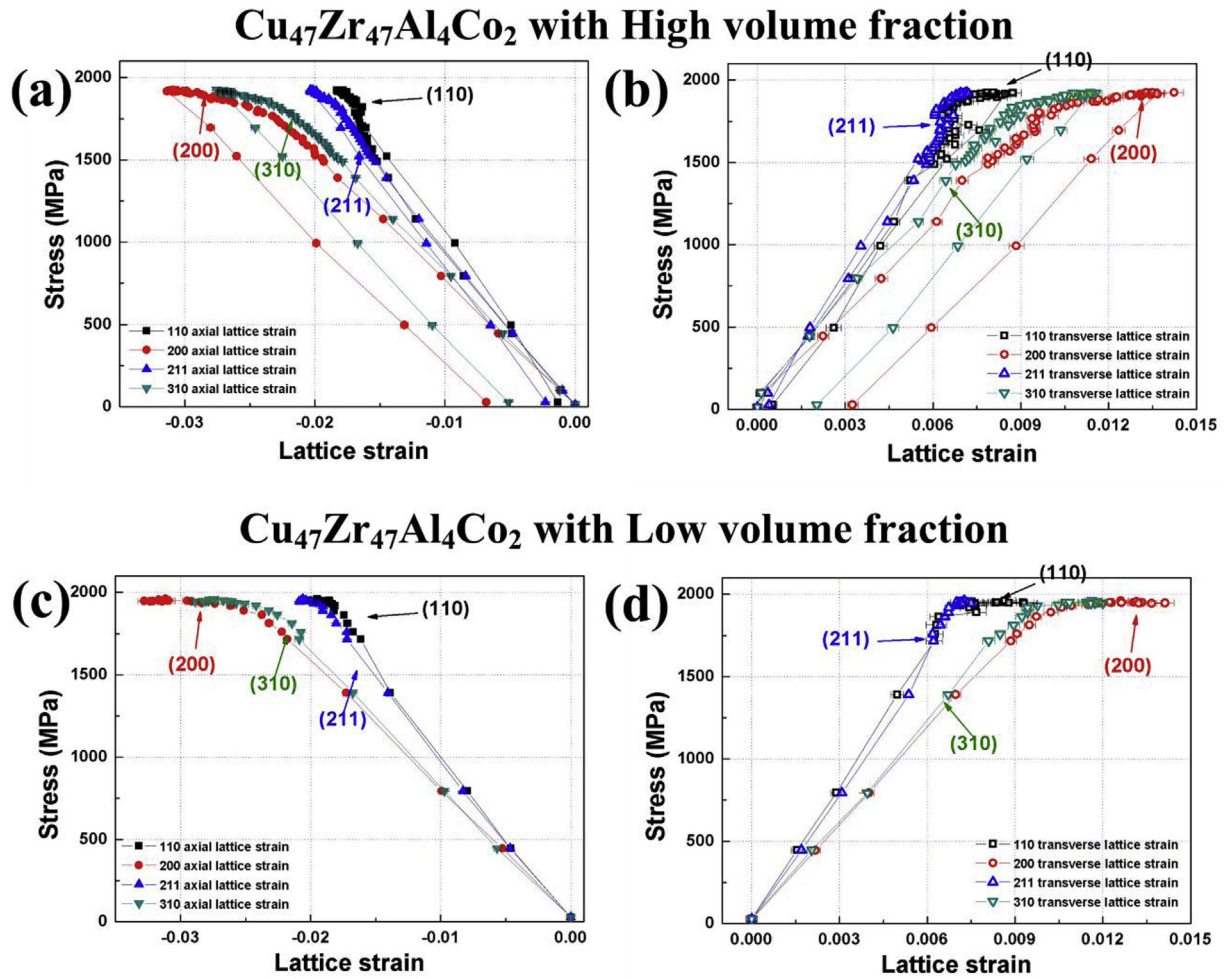


Fig. 5. The response of (hkl) plane-specific lattice strains along the (a)–(c) axial and (b)–(d) transverse directions as a function of applied stress for (a)–(b) HVF and (c)–(d) LVF BMG composites.

respectively. Due to limited potency of the martensitic transformation and glassy diffuse pattern, the threshold stress necessary for the onset of the martensitic transformation could be less than the stress level observed in the ND patterns. Recently, a systematic investigation using in-situ X-ray diffraction has been conducted regarding martensitic transformation of Ti-based BMG composites containing ductile dendritic phase during deformation, and reported that the transformation from the beta Ti phase to martensitic phase occurs during macroscopic elastic deformation [41]. Additionally, the slight increase in the gradient of the (110) lattice strain in Fig. 5 is observed around 1500 MPa for both LVF and

HVF samples. This stress range associated with the gradient increase seems to correspond to the martensitic transformation. Based on the previous studies [36,42], the deviation from the linear response of the elastic strain could be related to phase transformation and elastic-plastic transition (yielding behavior). Thus, this gradient increase could result mainly from the martensitic transformation, as shown in Fig. 6(a). As the volume fraction of the martensitic phases increases, they play a role in sharing the load, more specifically, taking more loads, because the martensitic phases are much stiffer [19,43]. It is also believed that the extent of martensitic transformation has a strong influence on the slope of

Table 3

Elastic anisotropy factor (A_{hkl}) and orientation-dependent diffraction elastic modulus (E_{hkl} , unit: GPa) along the axial and transverse directions for the HVF and LVF BMG composites. The (200), (310), (110), and (211) planes are calculated from the linear slope of the elastic strain vs. stress curves.

Orientation		(200)	(310)	(110)	(211)
Axial direction	A_{hkl}	0	0.09	0.25	0.25
	E_{hkl} (GPa)	76.600	82.507	94.994	96.413
	For HVF	(0.480)	(0.640)	(1.680)	(0.936)
	E_{hkl} (GPa)	77.780	81.776	103.503 (3.562)	98.660
Transverse direction	For LVF	(0.703)	(1.225)		(1.778)
	A_{hkl}	(200)	(310)	(110)	(211)
	E_{hkl} (GPa)	187.315 (5.999)	205.275 (6.587)	247.347 (11.218)	256.706 (2.038)
	For HVF				
	E_{hkl} (GPa)	192.168 (2.180)	207.091 (4.346)	271.941 (2.697)	267.252 (9.341)
	For LVF				

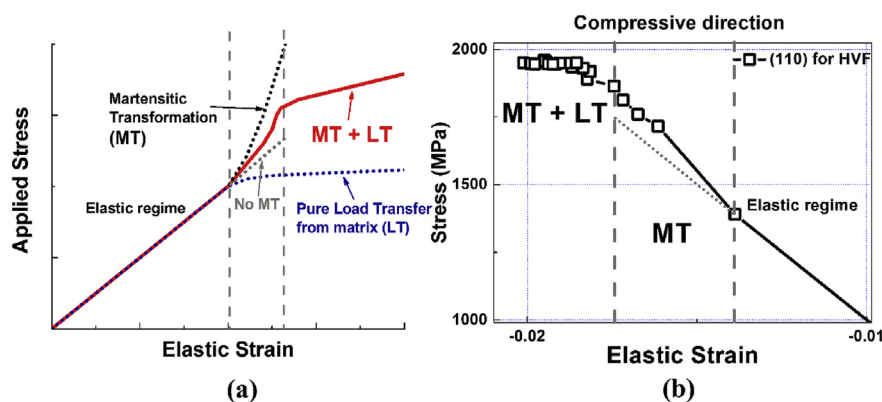


Fig. 6. (a) Schematic illustration of the variation of B2 phase elastic strain according to martensitic transformation (MT), load transfer from the glassy matrix (LT), and the cooperative MT and LT. (b) Enlarged curve of the elastic strain vs. stress for (110)_{B2} of the HVF along the compressive direction.

the stress-elastic strain curve, for example, the limited transformation leads to a less increase in the slope as shown in the red curve of Fig. 6(a).

The potency of martensitic transformation can be tailored by alloying addition, which is associated with the stacking fault energy (SFE) [44]. It has been reported that minor addition of alloying elements, such as Co, Ti, Fe, Ni, Ta, Cr, Ga, Hf, Nb, Ta and Ag, alter the SFE of the B2 CP in CuZr-based BMG composites. Specifically, the addition of 0.5% Co drastically lowers the SFE, which facilitates the phase transformation, and thus improves the mechanical properties, such as tensile ductility and hardening capability [44]. However, the present alloy consists of higher amount of Co (2.0%) and exhibits a limited work hardening capability, which are closely related to martensitic transformation, as compared to other 0.5% Co containing B2-CP reinforced BMG composites [19,31]. For example, the onset of martensitic transformation is observed around at 1500 MPa based on the elastic strain vs. stress behavior [Fig. 6(b)], which is much higher than other CuZr-based BMG composites (500–1000 MPa) [31]. More specifically, the previous study regarding the 0.5 at.% containing CuZr based BMG composite with 75 vol.% of the B2 CP, which is fairly close to that of the current HVF BMG composite, revealed that the martensitic transformation plays a dominant role in the microscopic deformation behavior, as revealed by the pronounced two yielding phenomena in the lattice strain evolution [31]. This behavior is not pronounced in the current study, indicating the limited martensitic transformation under the similar volume fraction. Also, the LVF BMG composite with the lower volume fraction (45–55 vol %) than HVF possesses deteriorated plasticity as compared to the HVF BMG composite, which is believed to be due to the influence of the lower volume fraction of CP, thus reduced potency of martensitic transformation. Based on the comparison between previous and present results, it is believed that the optimization of the SFE depends not only on the selection of minor alloying elements but also on the chemical composition. Therefore, the limited martensitic transformation in the present alloys, which results in the low ductility and hardening capability, could be a result of the excessive addition of Co, and the systematic tuning of the minor alloying elements is crucial to further improve the mechanical properties of the martensitic transformation mediated B2-CP reinforced BMG composites.

5. Conclusions

The microscopic deformation behavior of the 2.0% Co containing CuZr-based BMG composites reinforced by the B2-type CuZr CP with different volume fraction was investigated via in-situ neutron

experiments. Three deformation stages are revealed by the elastic-strain in the B2 CP; elastic, martensitic transformation, and load transfer regimes. The linear elastic strain response is followed by the martensitic transformation. The martensitic transformation from the B2 to B19' CPs is significantly suppressed, and a limited increase in the volume fraction of the B19' CP is observed. This limited martensitic transformation results in the deterioration of the work-hardening capability and overall plastic deformability, which are associated with the excessive addition of Co, as compared to other 0.5% Co containing CuZr-based BMG composites. In the subsequent loading, the clear load transfer from the glass matrix to B2 CP occurs, which indicates that the B2 CP takes the additional load due to shear banding deformation in the glassy matrix.

Additional information

Competing financial interests: The authors declare that they have no competing financial interests.

Acknowledgements

The in-situ neutron experiments at ORNL's Spallation Neutron Source was sponsored by the Scientific User Facilities Division, Office of Basic Energy Sciences, U.S. Department of Energy. We would like to acknowledge the support of the Department of Energy (DOE), Office of Fossil Energy, National Energy Technology Laboratory (DE-FE-0008855, DE-FE-0024054, and DE-FE-0011194), with Mr. V. Cedro, Mr. R. Dunst, Dr. P. Rawls, and Dr. J. Mullen as program managers. We very much appreciate the support of the U.S. Army Research Office project (W911NF-13-1-0438) with the program manager, Dr. D. M. Stepp. We thank the support from the National Science Foundation (DMR-1611180) with the program director, Dr. D. Farkas. We would like to thank QuesTek Innovations LLC under Award No. DE-SC0013220 with Dr. J. Saal as the program manager.

References

- [1] A.L. Greer, *Metallic glasses*, Science 267 (1995) 1947.
- [2] M. Ashby, A. Greer, *Metallic glasses as structural materials*, Scr. Mater. 54 (2006) 321–326.
- [3] W.L. Johnson, *Bulk glass-forming metallic alloys: Science and technology*, MRS Bull. 24 (1999) 42–56.
- [4] M.K. Miller, P. Liaw, *Bulk Metallic Glasses: an Overview*, Springer Science & Business Media, 2007.
- [5] Z.F. Zhang, J. Eckert, L. Schultz, *Difference in compressive and tensile fracture mechanisms of Zr₅₉Cu₂₀Al₁₀Ni₈Ti₃ bulk metallic glass*, Acta Mater. 51

- (2003) 1167–1179.
- [6] C.A. Schuh, T.C. Huftagel, U. Ramamurty, Mechanical behavior of amorphous alloys, *Acta Mater.* 55 (2007) 4067–4109.
 - [7] C.C. Hays, C.P. Kim, W.L. Johnson, Microstructure controlled shear band pattern formation and enhanced plasticity of bulk metallic glasses containing in situ formed ductile phase dendrite dispersions, *Phys. Rev. Lett.* 84 (2000) 2901–2904.
 - [8] D.C. Hofmann, J.Y. Suh, A. Wiest, G. Duan, M.L. Lind, M.D. Demetriou, W.L. Johnson, Designing metallic glass matrix composites with high toughness and tensile ductility, *Nature* 451 (2008) 1085–1089.
 - [9] J.W. Qiao, S. Wang, Y. Zhang, P.K. Liaw, G.L. Chen, Large plasticity and tensile necking of Zr-based bulk-metallic-glass-matrix composites synthesized by the bridgman solidification, *Appl. Phys. Lett.* 94 (2009) 151905.
 - [10] J. Qiao, H. Jia, P.K. Liaw, Metallic glass matrix composites, *Mater. Sci. Eng. R.* 100 (2016) 1–69.
 - [11] Z. Zhu, H. Zhang, Z. Hu, W. Zhang, A. Inoue, Ta-particulate reinforced Zr-based bulk metallic glass matrix composite with tensile plasticity, *Scr. Mater.* 62 (2010) 278–281.
 - [12] S. Pauly, J. Das, J. Bednarcik, N. Mattern, K.B. Kim, D.H. Kim, J. Eckert, Deformation-induced martensitic transformation in Cu-Zr-(Al,Ti) bulk metallic glass composites, *Scr. Mater.* 60 (2009) 431–434.
 - [13] Y. Wu, H. Wang, H.H. Wu, Z.Y. Zhang, X.D. Hui, G.L. Chen, D. Ma, X.L. Wang, Z.P. Lu, Formation of Cu-Zr-Al bulk metallic glass composites with improved tensile properties, *Acta Mater.* 59 (2011) 2928–2936.
 - [14] K.K. Song, S. Pauly, Y. Zhang, R. Li, S. Gorantla, N. Narayanan, U. Kühn, T. Gemming, J. Eckert, Triple yielding and deformation mechanisms in metastable Cu₄₇Zr_{47.5}Al₅ composites, *Acta Mater.* 60 (2012) 6000–6012.
 - [15] Z. Liu, R. Li, G. Liu, W. Su, H. Wang, Y. Li, M. Shi, X. Luo, G. Wu, T. Zhang, Microstructural tailoring and improvement of mechanical properties in CuZr-based bulk metallic glass composites, *Acta Mater.* 60 (2012) 3128–3139.
 - [16] Y.S. Oh, C.P. Kim, S. Lee, N.J. Kim, Microstructure and tensile properties of high-strength high-ductility Ti-based amorphous matrix composites containing ductile dendrites, *Acta Mater.* 59 (2011) 7277–7286.
 - [17] S.H. Hong, J.T. Kim, M.W. Lee, J.M. Park, M.H. Lee, B.S. Kim, J.Y. Park, Y. Seo, J.Y. Suh, P. Yu, Combinatorial influence of bimodal size of B2 TiCu compounds on plasticity of Ti-Cu-Ni-Zr-Sn-Si bulk metallic glass composites, *Metall. Mater. Trans. A* 45 (2014) 2376–2381.
 - [18] D.C. Hofmann, Shape memory bulk metallic glass composites, *Science* 329 (2010) 1294–1295.
 - [19] Y. Wu, Y. Xiao, G. Chen, C.T. Liu, Z. Lu, Bulk metallic glass composites with transformation-mediated work hardening and ductility, *Adv. Mater.* 22 (2010) 2770–2773.
 - [20] S.H. Hong, J.T. Kim, H.J. Park, J.Y. Suh, K.R. Lim, Y.S. Na, J.M. Park, K.B. Kim, Work-hardening and plastic deformation behavior of Ti-based bulk metallic glass composites with bimodal sized B2 particles, *Intermetallics* 62 (2015) 36–42.
 - [21] S. Hong, J. Kim, H. Park, Y. Kim, J. Suh, Y. Na, K. Lim, J. Park, K. Kim, Gradual martensitic transformation of B2 phase on TiCu-based bulk metallic glass composite during deformation, *Intermetallics* 75 (2016) 1–7.
 - [22] K. An, H.D. Skorpenske, A.D. Stoica, D. Ma, X.-L. Wang, E. Cakmak, First in situ lattice strains measurements under load at VULCAN, *Metall. Mater. Trans. A* 42 (2011) 95–99.
 - [23] X.-L. Wang, T. Holden, G.Q. Rennich, A. Stoica, P.K. Liaw, H. Choo, C.R. Hubbard, VULCAN—the engineering diffractometer at the SNS, *Phys. Rev. B Condens. Matter* 385 (2006) 673–675.
 - [24] P.K. Liaw, H. Choo, R. Buchanan, C. Hubbard, X. Wang, Development of an in situ neutron-scattering facility for research and education in the mechanical behavior of materials, *Mater. Sci. Eng. A* 437 (2006) 126–133.
 - [25] G.M. Stoica, A.D. Stoica, M.K. Miller, D. Ma, Temperature-dependent elastic anisotropy and mesoscale deformation in a nanostructured ferritic alloy, *Nat. Commun.* 5 (2014) 1–8.
 - [26] Y.-D. Wang, H. Tian, A.D. Stoica, X.-L. Wang, P.K. Liaw, J.W. Richardson, The development of grain-orientation-dependent residual stress in a cyclically deformed alloy, *Nat. Mater.* 2 (2003) 101–106.
 - [27] M.R. Daymond, M. Preuss, B. Clausen, Evidence of variation in slip mode in a polycrystalline nickel-base superalloy with change in temperature from neutron diffraction strain measurements, *Acta Mater.* 55 (2007) 3089–3102.
 - [28] M.R. Daymond, H.G. Priesmeyer, Elastoplastic deformation of ferritic steel and cementite studied by neutron diffraction and self-consistent modelling, *Acta Mater.* 50 (2002) 1613–1626.
 - [29] B.M.B. Grant, E.M. Francis, J. Quinta da Fonseca, M.R. Daymond, M. Preuss, Deformation behaviour of an advanced nickel-based superalloy studied by neutron diffraction and electron microscopy, *Acta Mater.* 60 (2012) 6829–6841.
 - [30] K. An, VDRIVE-data Reduction and Interactive Visualization Software for Event Mode Neutron Diffraction, ORNL Report No. ORNL-TM-2012-621, Oak Ridge National Laboratory, Oak Ridge, TN, 2012.
 - [31] Y. Wu, D. Ma, Q. Li, A. Stoica, W. Song, H. Wang, X. Liu, G. Stoica, G. Wang, K. An, Transformation-induced plasticity in bulk metallic glass composites evidenced by in-situ neutron diffraction, *Acta Mater.* 124 (2017) 478–488.
 - [32] J.F. Nye, *Physical Properties of Crystals: Their Representation by Tensors and Matrices*, Oxford University Press, 1985, pp. 143–145.
 - [33] M.T. Hutchings, P.J. Withers, T.M. Holden, T. Lorentzen, *Introduction to the Characterization of Residual Stress by Neutron Diffraction*, CRC Press, 2005, pp. 216–218.
 - [34] H.J. Stone, T.M. Holden, R.C. Reed, On the generation of microstrains during the plastic deformation of Waspaloy, *Acta Mater.* 47 (1999) 4435–4448.
 - [35] G. Song, Z. Sun, L. Li, X. Xu, M. Rawlings, C.H. Liebscher, B. Clausen, J. Poplawsky, D.N. Leonard, S. Huang, Z. Teng, C.T. Liu, M.D. Asta, Y. Gao, D.C. Dunand, G. Ghosh, M. Chen, M.E. Fine, P.K. Liaw, Ferritic alloy with extreme creep resistance via coherent hierarchical precipitates, *Sci. Rep.* 5 (2015) 16327.
 - [36] S. Huang, Y. Gao, K. An, L. Zheng, W. Wu, Z. Teng, P.K. Liaw, Deformation mechanisms in a precipitation-strengthened ferritic superalloy revealed by in situ neutron diffraction studies at elevated temperatures, *Acta Mater.* 83 (2015) 137–148.
 - [37] D. Wang, J. Mu, Y. Chen, Y. Qi, W. Wu, Y. Wang, H. Xu, H. Zhang, K. An, A study of stress-induced phase transformation and micromechanical behavior of CuZr-based alloy by in-situ neutron diffraction, *J. Alloys Compd.* 696 (2017) 1096–1104.
 - [38] N. Shi, M.A.M. Bourke, J.A. Roberts, J.E. Allison, Phase-stress partition during uniaxial tensile loading of a TiC-particulate-reinforced Al composite, *Metall. Mater. Trans. A* 28 (1997) 2741–2753.
 - [39] E.M. Francis, B.M.B. Grant, J.Q.d. Fonseca, P.J. Phillips, M.J. Mills, M.R. Daymond, M. Preuss, High-temperature deformation mechanisms in a polycrystalline nickel-base superalloy studied by neutron diffraction and electron microscopy, *Acta Mater.* 74 (2014) 18–29.
 - [40] G. Chen, H. Bei, Y. Cao, A. Gali, C.T. Liu, E.P. George, Enhanced plasticity in a Zr-based bulk metallic glass composite with in situ formed intermetallic phases, *Appl. Phys. Lett.* 95 (2009).
 - [41] J. Mu, Z. Zhu, R. Su, Y. Wang, H. Zhang, Y. Ren, In situ high-energy X-ray diffraction studies of deformation-induced phase transformation in Ti-based amorphous alloy composites containing ductile dendrites, *Acta Mater.* 61 (2013) 5008–5017.
 - [42] M.L. Young, M.F.X. Wagner, J. Frenzel, W.W. Schmahl, G. Eggeler, Phase volume fractions and strain measurements in an ultrafine-grained NiTi shape-memory alloy during tensile loading, *Acta Mater.* 58 (2010) 2344–2354.
 - [43] M. Thomasová, H. Seiner, P. Sedláček, M. Frost, M. Ševčík, I. Szurman, R. Kocich, J. Drahokoupil, P. Šittner, M. Landa, Evolution of macroscopic elastic moduli of martensitic polycrystalline NiTi and NiTiCu shape memory alloys with pseudo-plastic straining, *Acta Mater.* 123 (2017) 146–156.
 - [44] Y. Wu, D. Zhou, W. Song, H. Wang, Z. Zhang, D. Ma, X. Wang, Z. Lu, Ductilizing bulk metallic glass composite by tailoring stacking fault energy, *Phys. Rev. Lett.* 109 (2012) 245506.